A dynamic fatigue study of soda–lime silicate and borosilicate glasses using small scale indentation flaws

T. P. Dabbs, B. R. Lawn & P. L. Kelly*

Department of Applied Physics, School of Physics, University of New South Wales, Kensington, N.S.W. 2033, Australia

Manuscript received 27 July 1981

The dynamic fatigue characteristics of two glasses, soda–lime silicate and borosilicate, in water have been studied using a controlled indentation flaw technique. It is argued that the indentation approach offers several advantages over more conventional fatigue testing procedures: (i) the reproducibility of data is relatively high, eliminating statistics as a basis of analysis; (ii) the flaw ultimately responsible for failure is well defined and may be conveniently characterised before and after (and during, if necessary) the strength test; (iii) via adjustment of the indentation load, the size of the flaw can be suitably predetermined. Particular attention is devoted to the third point because of the facility it provides for systematic investigation of the range of flaw sizes over which macroscopic crack behaviour remains applicable.

The first part of the paper summarises the essential fracture mechanics theory of the extension of an indentation flaw to failure. A distinctive feature of this theory is the explicit incorporation of a residual contact term associated with elastic/plastic mismatch stresses in the indentation processes into the stress intensity factor for the growing crack. A scheme is thus devised whereby the indentation load is treated as a key test variable in the construction of universal dynamic fatigue curves. It is demonstrated that basic kinetic fracture parameters, relating to the crack velocity functions for macroscopic cracks, may be obtained in the usual way from slope and intercept measurements on plots of strength against stress rate; accommodation of the residual stress term is achieved via simple 'transformation' relations for converting 'apparent' kinetic parameters (i.e. evaluated on the basis of a flaw with no residual stress) to 'true' values.

In the next part of the paper the results of dynamic fatigue tests on glass rods in distilled water are described. Data are obtained for Vickers indentation loads in the range 0·05–100 N, corresponding to contact dimensions of 2–100 μm. The data fall on universal fatigue curves, within experimental scatter, as predicted. Evaluations of kinetic fracture parameters from these curves are consistent with those from independent determinations by other workers using macroscopic crack configurations.

Finally, the implications of the results in relation to the response of 'natural' flaws are discussed. It is suggested that flaws in the sub-micrometre domain could be of a nature somewhat different to that of true microcracks. Larger flaws, in the size range covered here, appear to behave as macroscopic cracks, provided account is taken of the crack driving force associated with residual stress fields. The residual term is shown to have a vital influence on the mechanics to failure; ignoring this term can lead to serious errors in evaluations of the parameters from fatigue data. This influence is manifest in borosilicate as well as soda–lime glass, even though the former is 'anomalous' in its indentation deformation properties, with significantly reduced susceptibility to elastic/plastic mismatch processes.

Numerous recent studies have provided compelling evidence that fracture mechanics data on macroscopic cracks can be used to predict the fatigue properties of glasses and other ceramics.[1–7] The underlying basis of the fracture mechanics approach is that fatigue failure occurs from rate dependent, subcritical extension of a microscopic flaw to an instability configuration; it is implied that the flaw is simply a scaled down version of the well defined macrocrack. Analysis of the strength characteristics under fatigue conditions then follows from two basic starting equations for the crack propagation: the first equation represents the driving force on the crack, $K \sim \sigma c^{1/2}$, where K is a stress intensity factor, σ is a uniform applied tensile stress, and c is a characteristic crack dimension; the second equation represents the ensuing stress enhanced motion of the crack, $v = v(K)$, where $v(K)$ is a crack velocity function. In principle, once the parameters of these two equations have been determined from controlled fracture specimens, the foundation is laid for the analytical prediction of fatigue response over a seemingly unlimited range of service conditions.

However, the fracture mechanics approach to the fatigue problem is not without its difficulties. For a

*Now at Fracture and Deformation Division, National Bureau of Standards, Washington, DC 20234, USA.

start, there is the statistical aspect of strength properties. Strength measures a combination of intrinsic toughness and flaw size, and the latter quantity is subject to considerable variability in the typical brittle material. It is accordingly necessary to test large sample populations to obtain reliable parameters for prediction purposes. Some attempts have been made to circumvent this difficulty by introducing controlled abrasion flaws into the test surfaces.[8] This procedure, although improving the reproducibility of results, nevertheless does not allow for *a priori* characterisation of the critical flaw; apart from the problem of quantifying the growth history of any individual abrasion flaw, it is generally not possible to specify which flaw will ultimately cause the failure.

A second difficulty concerns the assumed forms of the starting fracture mechanics equations mentioned above. The crack velocity function $v(K)$ has been subjected to particular scrutiny in this regard. It is common for this function to show more than one distinctive region of behaviour, corresponding to changes in rate controlling mechanism in a given material/environment system, although there is some doubt as to whether this is likely to be of significant influence in fatigue behaviour;[3,9] the region of lowest velocities (region I), governed by reaction kinetics at the crack tip, is expected to be dominant in the determinations of times to failure. On the other hand, knowledge of the exact analytical form of the velocity function in this region is vitally important when extrapolating short term data to the long lifetime domain;[10] in this context it needs to be noted that the $v(K)$ equations in general use are empirically based. But it is not only the crack velocity function which requires qualification. The simplistic relation $K \sim \sigma c^{1/2}$ must be seen as a special case (the 'Griffith limit') of a more general configuration where the forces initially responsible for creating the flaw persist (in whole or in part) to augment the ensuing crack propagation force.[11] Studies of indentation induced cracks in glass in these laboratories[12,13] have provided a convenient model 'flaw' system for quantifying residual stress effects of this kind. A sharp contact geometry is used to create a highly localised region of irreversible deformation, from which the cracks generate. It then becomes necessary to add an appropriate residual term to the stress intensity factor for crack propagation to allow for elastic/plastic mismatch contributions to the fracture driving force.[14] If ignored in fatigue analyses, the residual term can lead to large discrepancies between predicted and observed strength characteristics.[15,16]

A third difficulty with the fracture mechanics approach relates to the scale of the flaw. Do the laws of macroscopic crack growth continue to apply at the level of the typical flaw? There is now some evidence, particularly from studies on ultra high strength optical fibres,[17,18] to suggest that the entire nature of flaws in glass changes as the scale is reduced below some critical level. This is consistent with the concept of a threshold for development of well defined microcracks in concentrated stress fields,[19] a concept fully borne out by analysis of indentation flaw initiation in a wide range of brittle materials.[20,21] Extrapolation into the ultra high strength domain is therefore subject to an element of uncertainty, requiring that due attention be paid to potentially significant departures from the conventional mechanics of fatigue failure.

The present paper describes a study of the dynamic fatigue characteristics of the glass/water system, using the indentation flaw technique as a means of circumventing the major difficulties just described. Indentation patterns are generally highly reproducible, in which case the statistical element of strength measurement is conveniently eliminated, thereby allowing for accurate evaluation of materials. Moreover, the failure site is identified beforehand, so one may follow the crack evolution throughout the test sequence. With this facility, it is possible to investigate the factors which contribute to the basic fracture mechanics equations; the important contribution of residual stress effects to the stress intensity factor is a case in point which has already been mentioned. Finally, since the scale of the indentation event is readily amenable to strict control via the contact load, the way is open for establishing the range of validity of macroscopic crack laws. This last point forms one of the major thrusts of the work to be described below. In this sense our study may be seen as an extension of earlier indentation fatigue analyses of the glass/water system.[15,16] However, a somewhat simplified experimental procedure, based on a more recently developed theoretical description,[22] is adopted here. Further, in addition to the soda–lime glass type used previously, a borosilicate glass is also analysed. Apart from providing a wider base for comparison with results from other workers,[23-25] the latter glass type, which is 'anomalous' in the indentation deformation response,[26] affords the opportunity for investigating a material somewhat removed from the idealised stereotype assumed in the theoretical derivations.

Theoretical background

Vickers induced radial crack system as strength controlling flaw

We summarise here the essential features of the general theory of dynamic fatigue for indentation flaws,[22] with additional attention to the role of the scale of contact, as determined by the indentation load, as a test variable. Simplicity in the experimental test programme and in the ensuing analysis of the data is a key consideration in the formulation of the problem. To facilitate this simplicity, it is necessary to incorporate some ostensibly complicating elements into the mathematical derivations, notably a residual contact term.

A schematic of the model indentation flaw system is shown in Figure 1.[21] The pattern corresponds to that produced by a standard Vickers diamond pyramid indenter used in routine hardness testing. At a peak load, P, the pattern has characteristic surface dimensions, a_0 representing a central ('plastic') deformation zone and c_0 representing the radial traces of as-

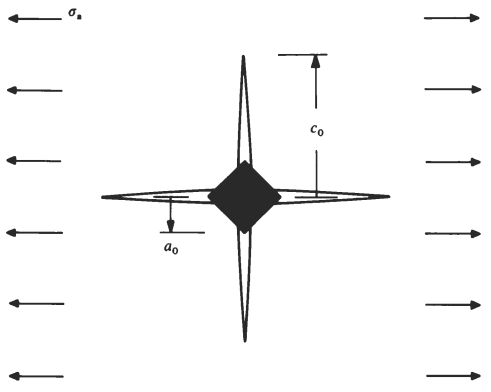

Figure 1. *Schematic surface view of deformation/fracture pattern produced by a Vickers indenter showing the characteristic radial crack dimension, c_0, the hardness impression dimension, a_0, and the subsequent applied tensile stress, σ_a. The driving force for radial crack system determined by peak indentation load, P, is not indicated.*

sociated cracks. The dimension a_0 is a measure of the resistance to irreversible deformation, and relates to P via the material hardness, H, defined as the mean contact pressure, by

$$a_0 = (P/2H)^{1/2}. \tag{1}$$

Similarly, the dimension c_0 is a measure of the resistance to crack propagation and relates to P via the material toughness, K_c, the critical stress intensity factor for crack extension under conditions of mechanical equilibrium, by

$$c_0 = (\chi_r P/K_c)^{2/3} \tag{2}$$

where χ_r is a geometrical (material dependent[14]) parameter. Comparison of the dimensions in Equations (1) and (2) affords a useful measure of material 'brittleness';[21] the region $c_0 \lesssim a_0$ is of particular interest in the context of the present work, for it signifies that the flaw must be encompassed within the deformation zone, corresponding to the sub-threshold realm of crack initiation. The effect of the deformation zone on the crack development is not confined to this region, however; it is found that well developed radial cracks in glass, i.e. at $c_0 \gg a_0$, remain well within the sphere of influence of the residual stress field (as revealed by birefringence[13]) centred about the contact area. In fact, the residual stress component of the indentation field is the source of the primary crack extension force, causing the radial crack to grow to its equilibrium size, c_0, during the unloading half cycle.[14] An important manifestation of this residual stress component is the continued, slow crack growth that is observed in glass after completion of the contact cycle;[13] this growth, activated by atmospheric moisture, takes the crack to some non-equilibrium configuration, say, $c_0' > c_0$.

Consider now the response of the radial crack flaw at c_0' to a subsequently applied uniform tensile stress σ_a. The stress intensity factor for the crack must now contain two components[12,13]

$$K = \chi_r P/c^{3/2} + \sigma_a(\pi\Omega c)^{1/2} \qquad (c \geqslant c_0') \tag{3}$$

where Ω is another geometrical parameter. We may note that Equation (2) follows from Equation (3) if we insert the equilibrium requirements $K = K_c$ and $c_0' = c_0$ at the initial condition $\sigma_a = 0$. Also, at zero residual stress, $\chi_r = 0$, Equation (3) reduces to the special case of Griffith-like cracks. The strength is then determined as the level of applied stress, $\sigma_a = \sigma$, at which a configuration of unstable equilibrium is attained, i.e. at which the conditions $K = K_c$ and $dK/dc > 0$, are satisfied.

Inert strength

In any analysis of fatigue it is convenient to take the inert strength as a reference baseline. This is the strength that obtains in a truly inert environment such that no nonequilibrium crack extension occurs during stressing to failure; inert strengths may be effectively achieved by testing at fast load rates or at low temperatures. Accordingly, putting $K = K_c$ into Equation (3) and solving for the applied stress,[13]

$$\sigma_a = [K_c/(\pi\Omega c)^{1/2}][1 - \chi_r P/K_c c^{3/2}], \tag{4}$$

we may identify the inert strength $\sigma = \sigma_i = \sigma_m$ in terms of a maximum in the function $\sigma_a(c)$, corresponding to an instability in the function $K(c)$ in Equation (3), at (σ_m, c_m), where

$$c_m/P^{2/3} = 4^{2/3}[\chi_r/K_c]^{2/3} \tag{5a}$$

$$\sigma_m P^{1/3} = (3/4^{4/3})[K_c/(\pi\Omega)^{1/2}][K_c/\chi_r]^{1/3}. \tag{5b}$$

Physically, the presence of the maximum means that the crack will undergo a stage of precursor stable growth, from c_0' to c_m, prior to failure. As a corollary to this point, the condition $c_0' < c_m$ is a necessary proviso for identifying σ_i with σ_m. It may be noted that the critical configuration expressed by Equation (5) is totally independent of c_0' so that, within the confines of the proviso just mentioned, the inert strength is insensitive to the crack history between indentation and failure testing.

In this way σ_m and c_m serve as useful reference parameters for indentation flaws produced at any given load, P.[22] In our present case, where P is to be used as an important test variable, it may be seen from Equation (5) that the constant quantities $c_m/P^{2/3}$ and $\sigma_m P^{1/3}$ afford a more general basis for data reduction.

Dynamic fatigue strength

Let us now deal with the strength behaviour under dynamic fatigue conditions, i.e. stressing at a fixed rate, $\sigma_a = \dot{\sigma}_a t$ ($\dot{\sigma}_a$ constant), such that nonequilibrium crack extension occurs prior to failure. For glass, such nonequilibrium extension occurs because of the accessibility of the crack tip to moisture. Thus the approach to the final crack instability proceeds along some subcritical path, $K(c) < K_c$, in accordance with some specified crack velocity function, until Equation (4) is ultimately satisfied at $c = c_f > c_m$; the corresponding strength region $\sigma < \sigma_m$ appropriately defines the domain of dynamic fatigue. If we adopt as representative over the entire subcritical region, $0 < K < K_c$, the most commonly used crack velocity

function[10]

$$v = v_0(K/K_c)^n \tag{6}$$

where v_0 and n are kinetic constants for the given material/environment system, we obtain from Equation (1) the differential equation[15]

$$\dot{c}/v_0 = \{[\chi_r/K_c]P/c^{3/2} + [(\pi\Omega)^{1/2}/K_c]\dot{\sigma}_a c^{1/2} t\}^n. \tag{7}$$

This must generally be solved numerically for the time to failure, t_f, i.e. the time to take the crack from c_0' to c_f, for any given values of P and $\dot{\sigma}_a$; the strength $\sigma = \dot{\sigma}_a t_f$ then follows.

At this point it is useful to rewrite Equation (7) in terms of reduced variables and so avoid having to specify numerous adjustable quantities for integration to proceed. The reference parameters σ_m and c_m defined in the previous section are used as the basis for normalisation, thus:[22]

$$\boldsymbol{S}_a = \sigma_a/\sigma_m \tag{8a}$$

$$\boldsymbol{C} \equiv c/c_m \tag{8b}$$

$$\boldsymbol{T} \equiv tv_0/c_m. \tag{8c}$$

Equation (7) accordingly reduces to

$$\dot{\boldsymbol{C}} = (1/4\boldsymbol{C}^{3/2} + 3\dot{\boldsymbol{S}}_a\boldsymbol{C}^{1/2}\boldsymbol{T}/4)^n \tag{9}$$

where $\dot{\boldsymbol{C}} = \mathrm{d}\boldsymbol{C}/\mathrm{d}\boldsymbol{T}$ and $\dot{\boldsymbol{S}}_a = \boldsymbol{S}_a/\boldsymbol{T}$. Strictly, the time to failure $\boldsymbol{T}_f$ should be evaluated in terms of an initial crack size, $\boldsymbol{C}_0'$, and final crack size, $\boldsymbol{C}_f$ (>1, as determined by the condition $\dot{\boldsymbol{C}} = 1$). However, it can be shown that the integration is insensitive to the initial crack size in the range $\boldsymbol{C}_0 \leqslant \boldsymbol{C}_0' \leqslant \boldsymbol{C}_m$, where $\boldsymbol{C}_0 = 0{\cdot}397$, cf. Equations (2) and (5a), and $\boldsymbol{C}_m = 1$;[22] under such circumstances one may take $\boldsymbol{T} = 0$ and $\boldsymbol{C} = 0{\cdot}397$ as an invariant initial condition. It will be noted that Equation (9) contains no reduced variable corresponding to χ_r in Equation (7); the residual stress term has conveniently been incorporated into the reference crack dimension, c_m, in Equation (5a).

Thus for any fixed value of the kinetic constant, n, Equation (9) may be solved to generate the dynamic fatigue function, $\boldsymbol{S}(\dot{\boldsymbol{S}}_a)$.[22] When plotted in logarithmic coordinates these functions tend to linearity in the fatigue domain $\boldsymbol{S} < \boldsymbol{S}_i = 1$ (this tendency increasing with n), and may accordingly be represented by the usual kind of strength/stress rate relation[2–7]

$$\boldsymbol{S} = (\Lambda'\dot{\boldsymbol{S}}_a)^{1/(n'+1)} \tag{10}$$

where Λ' and n' are intercept and slope parameters; the primed notation is used here to remind us that we are dealing with solutions of the fatigue equations with the residual stress term included, so data analysis from as-indented specimens using Equation (10) in the conventional manner would yield 'apparent' values for the constants in the crack velocity function. Both Λ' and n' can be uniquely related to the 'true' crack velocity exponent, n, by means of empirical analysis of the numerical fits to Equation (10);[22]

$$n' = 0{\cdot}763\, n \tag{11a}$$

$$\Lambda' = 2{\cdot}51\, n^{0{\cdot}462}. \tag{11b}$$

Evaluation of fracture parameters from universal dynamic fatigue curves

Equation (10) lays the foundation for plotting dynamic fatigue data on universal curves, from which the true kinetic fracture constants may be evaluated. Taking note of the way in which the load variable, P, is displayed in Equation (5), we may write the normalised strength and stress rate from Equation (8) in the form

$$\boldsymbol{S} = \sigma/\sigma_m = \sigma P^{1/3}/[\sigma_m P^{1/3}] \tag{12a}$$

$$\dot{\boldsymbol{S}}_a = \dot{\sigma}_a c_m/\sigma_m v_0 = \dot{\sigma}_a P[(c_m/P^{2/3})/(\sigma_m P^{1/3})v_0] \tag{12b}$$

where the terms in square brackets are invariants for a given system. Then Equation (10) may be denormalised thus

$$\sigma P^{1/3} = (\lambda_P'\dot{\sigma}_a P)^{1/(n'+1)} \tag{13}$$

where

$$\lambda_P' = \Lambda'(\sigma_m P^{1/3})^{n'}(c_m/P^{2/3})/v_0. \tag{14}$$

Combination with Equation (11) then gives

$$n = 1{\cdot}31\, n' \tag{15a}$$

$$v_0 = 2{\cdot}84\, n'^{0{\cdot}462}(\sigma_m P^{1/3})^{n'}(c_m/P^{2/3})/\lambda_P'. \tag{15b}$$

It is estimated that Equation (15a) is accurate to $\approx 1\%$, and Equation (15b) to $\approx 10\%$, in the region $n > 10$[22] (which covers most brittle solids studied thus far).

Hence a complete characterisation of fatigue response may be obtained from a universal, linear plot of $\log(\sigma P^{1/3})$ against $\log(\dot{\sigma}_a P)$ over the load range of interest, together with appropriate inert strength determinations. The fracture parameters evaluated from such analysis may be expected to be representative of true macroscopic crack behaviour.

Experimental

Materials preparation and test procedure

Rod specimens of soda–lime silicate (wt% composition $69SiO_2$, $13Na_2O$, $4CaO$, $1B_2O_3$, $4Al_2O_3$, $2K_2O$, $4BaO$, $2MgO$, 1 other) and borosilicate ($81SiO_2$, $13B_2O_3$, $4Na_2O + K_2O$, $2Al_2O_3$) glass* were cut from 5 mm diameter cane into 215 mm lengths. All the rods were annealed, the soda–lime at 520°C and the borosilicate at 610°C, for 24 h to remove any existing surface stresses. They were then etched in a solution of 10% HF/10% H_2SO_4 for 6 min to nullify any large handling flaws.

Each rod was indented midway along its length with a standard Vickers indenter. Special care was taken to align the indenting pyramid symmetrically with respect to the rod, such that the impression diagonals (Figure 1) were oriented perpendicular and parallel to the rod axis. All such indentations were made in air, at a constant 10 s contact duration, using microhardness testing equipment covering a working load range 0·05–100 N. A microscopic examination

*Schott-Ruhrglas, GMBH.

was made of all indentation sites to ascertain first, whether crack initiation had occurred and second, the nature of the ensuing crack pattern. In accordance with a previous study,[26] radial crack formation was much better defined in the soda–lime than in the borosilicate specimens, the latter being complicated by the incidence of spurious ring cracks and a tendency for the radials to grow outward from points on the impression perimeter away from the corners. Bearing in mind our stated aim in this study to investigate the range of validity of macroscopic crack laws, the criterion for accepting any given specimen for subsequent strength testing was that there should be a reasonably well developed radial crack trace closely parallel to a rod circumference (thereby ensuring the existence of a suitable dominant flaw nearly normal to the designated tensile axis of the rod). For both glass types the minimum loading at which such a configuration obtained was of order 1 N, but for soda–lime glass this threshold could be reduced dramatically, to $<0{\cdot}05$ N, by immersing the newly indented surfaces in a solution of 1% HF/1% H_2SO_4 for ≈ 60 s; borosilicate remained immune to any such treatment. A more detailed description of this crack initiation process will be given elsewhere.[27]

The specimens which passed the above 'acceptance' test were then broken in four-point bending, using apparatus constructed in accordance with ASTM specifications,[28] with an inner span of 20 mm and an outer span of 60 mm. A crosshead testing machine was used to deliver the bending force, which was monitored at slow stress rates ($\lesssim 100$ MPa s^{-1}) by a conventional strain gauge instrumented load cell and at fast rates ($\gtrsim 100$ MPa s^{-1}) by a piezoelectric cell. Both cells gave a linear load/time response at constant crosshead speed; the stress at failure and the stress rate were then evaluated from this response using simple beam theory. The practical range of stress rates available with our equipment was 0·1–2000 MPa s^{-1}. To ensure that the indentation flaws were always located at the maximum tensile surface in the bending rig, a metal flag was attached to the end of each rod prior to indentation; it was then a simple matter of maintaining the flag vertical during the two stages of testing. The average interval between indentation and bending was ≈ 1 h, during which time the cracks were exposed to air (except, of course, for those specimens exposed to the post-indentation etch treatment mentioned above). During the bend test the crack environment was controlled to meet the requirements of equilibrium and nonequilibrium extension: inert environments were obtained either by blowing dry nitrogen gas through a plastic sleeve encasing the rod or by covering the indentation sites with a drop of silicone oil; the noninert environment was similarly obtained by covering the indentations with a drop of distilled water. All broken specimens were examined to confirm that failure had occurred from the indentation flaw; a few specimens broke from other origins (more frequently at the lower indentation loads) and these were deleted from the results. The post-indentation examinations served also to ensure that the crack dimensions at failure were sufficiently small, $\lesssim$ one-tenth of the rod diameter, for specimen size and shape effects to be neglected.

Before conducting the test runs proper, a preliminary check was made on soda–lime glass to investigate the strength characteristics of specimens containing cracks induced by post-indentation etching. It could be argued that such cracks might tend to be blunt and thereby give rise to higher strengths than appropriate to cracks produced in air. Accordingly, specimens were indented at $P = 0{\cdot}7$ N, at which load spontaneous crack 'pop-in' occurred in about one half of the cases; those apparently free from cracks were etched. Inert strengths were then measured for both groups, giving 136 ± 10 MPa (12 specimens) and 134 ± 10 MPa (16 specimens) respectively. Thus the crack severity is insensitive to the formation history.

Determination of inert strength parameters

Test runs were made in silicone oil and nitrogen gas environments to determine the inert strength parameters contained in Equation (5). In the case of the nitrogen tests the rods were prepared with three ostensibly identical indentations in their surfaces instead of the usual one, for reasons to be made clear below. To obtain the parameter in σ_m, the strengths were measured over a range of indentation loads and stress rates for both glasses. The results are shown in Figure 2, as a plot of $\sigma_i P^{1/3}$ against $\dot{\sigma}_a P$; this mode of graphical representation, based on the scheme for normalising fatigue curve coordinates in Equation (12), is useful for establishing the domain of truly inert strengths. The soda–lime rods do in fact show some tendency to fatigue at $\dot{\sigma}_a P \lesssim 100$ MPa s^{-1} N, indicating that the environments are not entirely free of moisture. The data points in Figure 2 represent means and standard deviations, in logarithmic coordinates, of 6–15 specimens. The average standard deviation is $\approx 8\%$, somewhat higher for borosilicate than for soda–lime glass.* Computation of the mean and standard deviation for all rods falling within the fatigue-free region of Figure 2 accordingly gives $\sigma_m P^{1/3} = 137 \pm 8$ MPa $N^{1/3}$ (87 specimens) for soda–lime glass and $\sigma_m P^{1/3} = 173 \pm 19$ MPa $N^{1/3}$ (129 specimens) for borosilicate glass.

Next, the specimens broken in nitrogen were examined optically to obtain the parameter in c_m in Equation (5).[22] For this purpose, surface trace measurements were made of the two indentation flaws which had survived each rod failure. It is argued that the radial cracks perpendicular to the tensile bend axis must have been taken very close to the instability configuration, and accordingly provide a measure of c_m. The radial cracks parallel to the tensile axis should, of course, be unaffected by the bending, and thus

*This compares with the 2–3% error obtainable in the biaxial testing of indented soda–lime glass plates, where specimen alignment difficulties can be effectively eliminated altogether.[29] The choice of rods rather than plates in this study is a reflection of our ultimate aim of expanding the test programme to the domain of optical fibres.

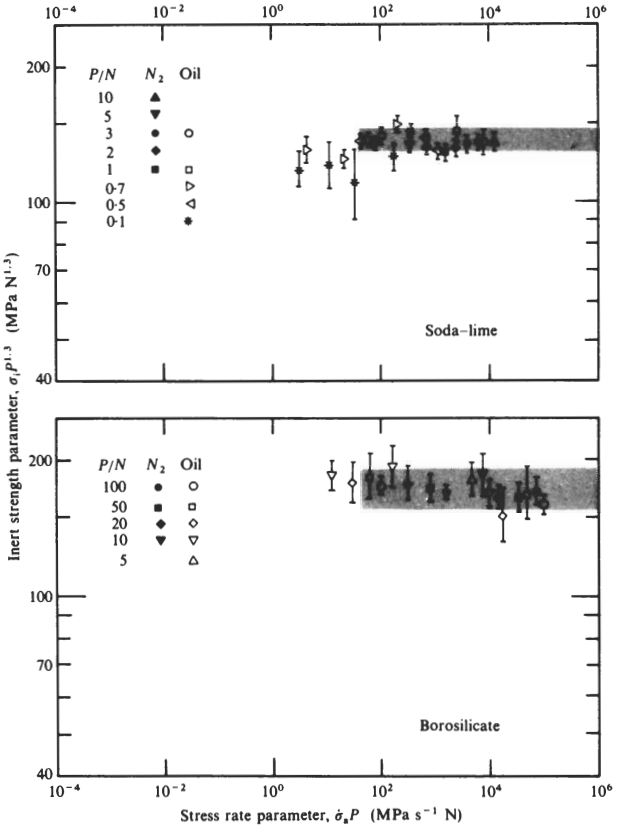

Figure 2. *Normalised inert strength data for soda–lime and borosilicate glasses tested in silicone oil and dry nitrogen at specified indentation loads. Shaded bands represent means and standard deviations of $\sigma_m P^{1/3}$ in the region of $\dot{\sigma}_a P$ considered to be free of all fatigue effects*

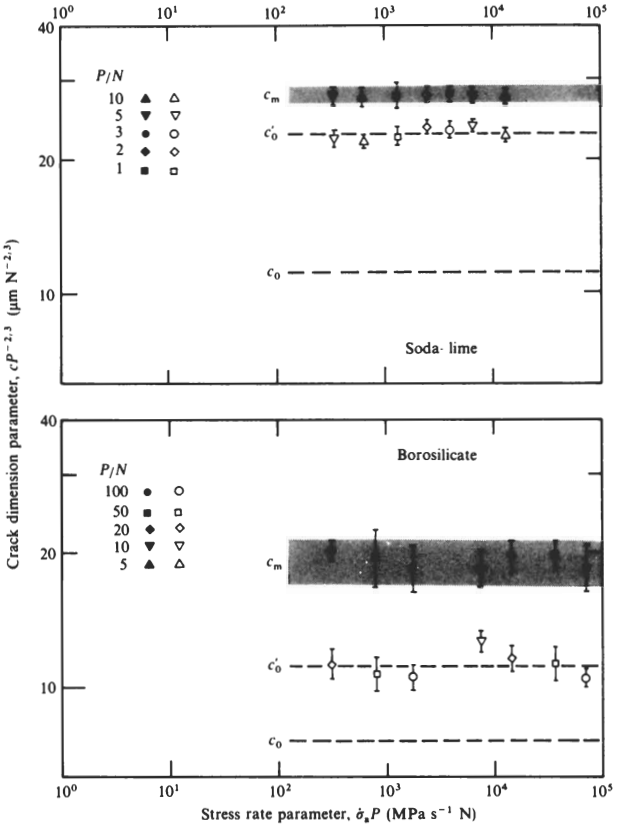

Figure 3. *Normalised crack dimension data for soda–lime and borosilicate glasses tested in dry nitrogen at specified indentation loads and at stress rates within the inert strength region (see Figure 2). Shaded bands represent means and standard deviations of $c_m/P^{2/3}$. The dashed line represents the mean of $c_0'/P^{2/3}$ data. Data satisfy condition $c_0 \leqslant c_0' \leqslant c_m$ everywhere, where c_0 is determined from Equations (2) and (5a) as 0·397 c_m.*

provide a measure of c_0'; measurements immediately before and after failure testing were made to confirm this expectation. The spacings between indentations in this particular series of tests were made sufficiently great relative to the maximum crack dimensions that interactions between neighbours could be completely disregarded. Figure 3 shows the results of the measurements; the use of $\dot{\sigma}_a P$ as abscissa in this Figure is simply to maintain consistency with the graphical scheme adopted for Figure 2, whereupon it is readily apparent that the crack size data are pertinent to the inert strength region. As in Figure 2, individual data points represent means and standard deviations, computed in logarithmic coordinates, of 6–15 specimens. It is immediately clear from the plots that the proviso $c_0' < c_m$ for identifying σ_i with σ_m in the derivation of Equation (5) is everywhere satisfied. Averaging over all rods gives the requisite quantities $c_m/P^{2/3} = 27{\cdot}9 \pm 1{\cdot}2$ μm $N^{-2/3}$ and $c_0'/P^{2/3} = 22{\cdot}6$ μm $N^{-2/3}$ (40 cracks) for soda–lime glass and $c_m/P^{2/3} = 19{\cdot}0 \pm 2{\cdot}2$ μm $N^{-2/3}$ and $c_0'/P^{2/3} = 11{\cdot}2$ μm $N^{-2/3}$ (35 cracks) for borosilicate glass, the relatively large standard deviation for the c_m parameter in the latter case reflecting the less well defined crack geometry alluded to in the previous subsection.

With these determinations, we obtain from Equation (5) the quantities $K_c/\chi_r = 27{\cdot}1 \pm 1{\cdot}8$ MPa $m^{1/2}$ and $K_c/(\pi\Omega)^{1/2} = 0{\cdot}97 \pm 0{\cdot}06$ MPa $m^{1/2}$ for soda–lime glass, and $K_c/\chi_r = 48{\cdot}3 \pm 8{\cdot}4$ MPa $m^{1/2}$ and $K_c/(\pi\Omega)^{1/2} = 1{\cdot}01 \pm 0{\cdot}12$ MPa $m^{1/2}$ for borosilicate glass. Noting that the two glasses have similar K_c values, ≈0·75 MPa $m^{1/2}$,[25,26] it is immediately clear that the level of residual stress, as measured by χ_r, is substantially smaller for borosilicate. On the other hand, the Ω parameter is similar for the two cases, suggesting that the essential penny-like characteristics of the radial crack system[14] do not vary much from glass to glass.

Analysis of dynamic fatigue results

In accordance with the procedure outlined in the previous section, dynamic fatigue data were obtained for both soda–lime and borosilicate glasses in water. The results are shown in Figure 4, as a logarithmic plot of $\sigma P^{1/3}$ against $\dot{\sigma}_a P$, covering the available range of indentation loads and stress rates. Within the experimental scatter, indicated here in the usual way by standard deviation bars for 6–15 specimens, there appears to be no systematic tendency for data at different loads to depart from universal behaviour. A significant fatigue effect is evident in both glasses, although the susceptibility is clearly less marked in the borosilicate.

Also included in Figure 4 are theoretical data fits, shown as the solid curves, computed as follows. First, a linear regression analysis, in logarithmic coordinates, was made of all the fatigue data, taking individual points rather than mean values. This gave slope and intercept terms (the latter expressed in terms of units indicated on the axes in Figure 4) from Equation (13), with standard errors: thus, $n' = 14{\cdot}0 \pm 0{\cdot}3$ and $\log \lambda'_P = 27{\cdot}9$ for soda–lime (128 specimens) and $n' = 27{\cdot}8 \pm 1{\cdot}9$ and $\log \lambda'_P = 57{\cdot}0$ for borosilicate (86 specimens). Next, taking Equation (15) in conjunction with the inert strength parameters determined in the previous section, the requisite kinetic parameters were evaluated: $n = 18{\cdot}4 \pm 0{\cdot}4$ and $\log (v_0/\mathrm{m\,s^{-1}}) = -1{\cdot}50$ for soda–lime and $n = 36{\cdot}4 \pm 2{\cdot}5$ and $\log (v_0/\mathrm{m\,s^{-1}}) = 1{\cdot}63$ for borosilicate. From these evaluations, along with the initial crack conditions expressed in the c'_0 curve in Figure 3, Equation (7) could be solved in absolute terms at specified P and $\dot{\sigma}_a$, for each of the glass types; the theoretical curves were thereby generated over the range of coordinates displayed in Figure 4.

It should be emphasised here that the computational procedure just outlined is not merely a curve-fitting exercise. The agreement obtained between the regenerated fatigue curves and the data points is a measure of the validity of the residual stress theory for contact induced flaws. To evaluate the parameters for insertion into Equation (7) we have had to invoke Equation (15) to transform 'apparent' kinetic parameters into 'true' kinetic parameters, as well as to obtain independent measurements of inert strength parameters. In addition, the theoretical derivations have been based on certain assumptions, such as the insensitivity of the 'universal fatigue curves' to initial crack conditions, and the dominance of region I crack velocity behaviour. All of these factors are potential contributors to uncertainty in theoretical prediction, and the results in Figure 4 need to be seen in this light.

The axes in Figure 4 could equally well have been expressed in terms of contact dimension, a_0, using measured hardness values, H, of $6{\cdot}6 \pm 0{\cdot}5$ GPa for soda–lime and $6{\cdot}5 \pm 0{\cdot}5$ GPa for borosilicate in Equation (1) to eliminate P, in order to introduce a spatial scaling coordinate into the description. For the load range 0·05–100 N covered by the data in the figure this corresponds to a dimension range 2–100 μm.

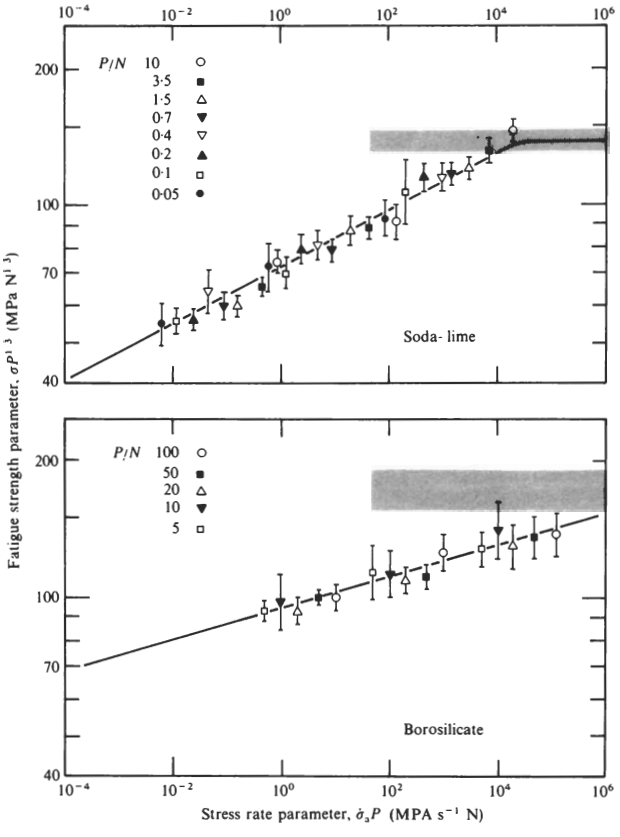

Figure 4. *Normalised dynamic fatigue data for soda–lime and borosilicate glasses in distilled water at specified indentation loads. Shaded bands represent inert strength limits determined from Figure 2. Solid curves are theoretical data fits*

Discussion

The indentation crack technique described here for investigating the dynamic fatigue properties of glasses offers certain unique advantages both as a tool for the evaluation of materials and as a model system for characterising flaw response. Insofar as the first of these two points is concerned, the simplicity of the experimental procedure, the economy in specimen usage, and the reproducibility of data are obvious virtues. As to the second point, the incorporation of a well defined residual contact component into the stress intensity factor provides for a generalisation of the Griffith flaw concept. It is implied that naturally occurring flaws may depart similarly from the idealised Griffith response.[15, 16, 30] A feature of the approach adopted here is that, by accommodating the complexities of an additional stress intensity component within the formal fracture mechanics framework, we avoid the need to remove the modifying element (in this case the residual stress field) physically from the indented surface prior to strength testing. From the mathematical viewpoint, the procedure for ultimately analysing the dynamic fatigue data is barely more complicated than that conventionally adopted; essentially, one major, additional step is involved, that of transforming 'apparent' into 'true' kinetic parameters. One further important advantage of using indentation flaws lies in our ability to predetermine the failure site, thereby allowing for quantitative characterisation of flaw severity (e.g. via P, c'_0, and c_m). Alternative methods of introducing controlled flaws, such as machining or abrasion,[8] are less amenable to such characterisation.[30]

The results for the two glass/water systems studied here may be readily compared, via the important susceptibility parameter, n, with those obtained on nominally similar systems by other workers. Wiederhorn[25] has systematically compiled crack velocity data from double cantilever test programmes, obtaining $n = 16$–19 for soda–lime and 31–37 for borosilicate

over many runs. Most other evaluations have been made using dynamic fatigue data from surfaces with relatively ill defined flaw characteristics; values obtained in the same strength region as covered in this work tend to span the range n' to n, i.e. 14·0–18·4 for soda–lime[2,9,23,24] and 27·6–36·0 for borosilicate.[23,24] This is sufficient agreement to suggest that macroscopic crack laws may usefully be applied to predict flaw response, provided first of all that the flaw does retain the nature of a true microcrack and second that proper account is taken of residual stress terms in the flaw driving force.

It is interesting to consider now the implications of the appearance of the indentation load (or the equivalent contact dimension) in the fatigue plot coordinates of Figure 4. We may note that the effect of varying P (or a_0) is simply to cause translation along the universal fatigue curve. In principle, therefore, one could generate a fatigue curve through variations in P alone (notwithstanding the limits in load range imposed by practical restrictions mentioned earlier), without ever having to vary $\dot{\sigma}_a$. Most far reaching, however, is the implication concerning the domain of validity of the macroscopic crack laws. Our results extend down toward $P \approx 0{\cdot}05$ N, $a_0 \approx 2$ μm (for soda–lime, somewhat higher for borosilicate), where the crack processes exhibit threshold behaviour. This threshold, as we have shown in the etching experiments, can be sensitive to prevailing conditions, and it is conceivable that it may be further depressed in favourable circumstances. However, at sufficiently low loads, corresponding to the submicrometre region of flaw sizes, we must expect that the entire form of the strength degrading contact flaw could be different from that described in the present work, in which case unconsidered application of conventional fracture mechanics formulations might lead to serious discrepancies in failure predictions. Since sub threshold flaws will inevitably be contained within the confines of the deformation zone responsible for ultimate crack initiation, the role of local concentrations of residual stress must be expected to be even greater than for macroscopic radial cracks. The allusion that flaws in this region of behaviour may not possess the distinguishing features of well defined microcracks should not, of course, be taken to imply that fatigue effects must be suppressed; optical fibres, for instance, exhibit significant fatigue at ultra high strengths.[17] However, the actual mechanics of fatigue are likely to be governed by processes of an origin quite different from that of crack propagation, in which case material parameters evaluated using the present fatigue analysis would have no physical significance. In this context, extension of the indentation method to the sub threshold load domain would appear to be a promising area for future systematic study.

It was indicated in the introduction to this paper that borosilicate glass is 'anomalous' in its indentation deformation response. Thus, whereas soda–lime glass, which has a 'normal' response, tends to deform by shear activated flow beneath the sharp indenter, borosilicate tends to a pressure activated densification mode. The latter mode is less disruptive to the glass network, and accordingly is not so effective in either creating the necessary flaw nuclei for initiating well defined radial cracks or producing residual stresses for driving these same cracks after the indentation is completed.[26] Intuitively, it might be thought that the level of residual stress in borosilicate or other like anomalous glasses could well be sufficiently small to render it of secondary importance in the crack driving force, whence the flaws would respond in the classical Griffith manner. The criterion for judging whether the residual component does indeed retain a vital role is simply that the crack should show some precursor stable growth to failure under inert conditions, i.e. that $c_0' < c_m$. Figure 3 confirms that this condition is met for the borosilicate as well as for the soda–lime glass, although the smaller values of both these crack dimensions in the former glass attests to a reduced residual stress intensity factor. It is suggested that satisfaction of the precursor growth condition should always be established before applying the fatigue analysis presented in this work to any given material/environment system, even in cases where the deformation properties are known to be entirely 'normal'; it is possible that the radial crack might, by virtue of some unusual post indentation circumstances (e.g. spurious mechanical or thermal impulses), grow beyond c_m prior to strength testing.[30] On the other hand, once the proviso has been verified, it is unnecessary to specify the actual level of residual stress itself; this information, it will be recalled from Equation (5a), is conveniently contained within the quantity c_m.

Finally, it will be noted that the dynamic fatigue data in Figure 4 follow a linear plot up to the inert strength levels, within the scatter bands of individual points. This would appear to justify the assumption of a single region crack velocity function in the fracture mechanics calculations; the effect of a second, transport controlled region at higher velocities would be apparent as a distinctive rise in the fatigue curve before levelling out at the inert strength plateau.[22] Apart from their small size, the indentation flaws tend to fail from their points of intersection with the specimen surface;[15] these factors can be expected to minimise the extent of transport limiting processes.[9] Our earlier suggestion that macroscopic cracks and microscopic (post threshold) flaws appear to be governed by the same kinetic equations, as dictated by the n parameter, is therefore subject to this kind of qualification.

Acknowledgements

The authors acknowledge funding through the Australian Research Grants Committee.

References

1. Wiederhorn, S. M. & Bolz, L. H. (1970). *J. Am. Ceram. Soc.* **53**, 543.
2. Evans, A. G. (1974). *Int. J. Fract.* **10**, 251.
3. Evans, A. G. & Johnson, H. (1975). *J. Mater. Sci.* **10**, 214.
4. Wiederhorn, S. M. (1975). *J. Non-Cryst. Solids* **19**, 169.
5. Wiederhorn, S. M. (1974). In *Ceramics for high performance applications,*

edited by J. J. Burke, A. E. Gorum & R. N. Katz. Brook Hill Publishing Co., Chestnut Hill, Mass.
6. Ritter, J. E. (1978). In *Fracture mechanics of ceramics*, edited by R. C. Bradt, D. P. H. Hasselman & F. F. Lange. Plenum, New York. Vol. 4, p. 667.
7. Pletka, B. J. & Wiederhorn, S. M. (1981). *J. Mater. Sci.* In press.
8. Mould, R. E. & Southwick, R. D. (1959). *J. Am. Ceram. Soc.* **42**, 542, 582.
9. Chandan, H. C., Bradt, R. C. & Rindone, G. E. (1978). *J. Am. Ceram. Soc.* **61**, 207.
10. Wiederhorn, S. M. & Ritter, J. E. (1979). In *Fracture mechanics applied to brittle materials*, edited by S. W. Freiman. ASTM Special Technical Publication 678, Philadelphia. P. 202.
11. Lawn, B. R. & Wilshaw, T. R. (1975). *Fracture of Brittle Solids*. Cambridge University Press, London. Ch. 2.
12. Lawn, B. R. & Marshall, D. B. (1979). *J. Am. Ceram. Soc.* **62**, 106.
13. Marshall, D. B. & Lawn, B. R. (1979). *J. Mater. Sci.* **14**, 2001.
Marshall, D. B., Lawn, B. R. & Chantikul, P. *Ibid*, 2225.
14. Lawn, B. R., Evans, A. G. & Marshall, D. B. (1980). *J. Am. Ceram. Soc.* **63**, 574.
15. Marshall, D. B. & Lawn, B. R. (1980). *J. Am. Ceram. Soc.* **63**, 532.
16. Chantikul, P., Lawn, B. R. & Marshall, D. B. (1981). *J. Am. Ceram. Soc.* In press.
17. Ritter, J. E. & Jakus, K. (1977). *J. Am. Ceram. Soc.* **60**, 171.
18. Dabbs, T. P., Marshall, D. B. & Lawn, B. R. (1980). *J. Am. Ceram. Soc.* **63**, 224.
19. Lange, F. F. (1978). In *Fracture mechanics of ceramics*, edited by R. C. Bradt, D. P. H. Hasselman & F. F. Lange. Plenum, New York. Vol. 4, p. 799.
20. Lawn, B. R. & Evans, A. G. (1977). *J. Mater. Sci.* **12**, 2195.
21. Lawn, B. R. & Marshall, D. B. (1979). *J. Am. Ceram. Soc.* **62**, 347.
22. Lawn, B. R., Marshall, D. B., Anstis, G. R. & Dabbs, T. P. (1981). *J. Mater. Sci.* In press.
Cook, R. F., Lawn, B. R. & Anstis, G. R., *J. Mater. Sci.* In press.
23. Ritter, J. E. & Sherburne, C. L. (1971). *J. Am. Ceram. Soc.* **54**, 601.
24. Ritter, J. E. & LaPorte, R. P. (1975). *J. Am. Ceram. Soc.* **58**, 265.
25. Wiederhorn, S. M. Unpublished work.
26. Arora, A., Marshall, D. B., Lawn, B. R. & Swain, M. V. (1979). *J. Non-Cryst. Solids* **31**, 415.
27. Dabbs, T. P. & Lawn, B. R. To be published.
28. ASTM Designation C158. (1976). In *Annual book of ASTM standards*. American Society for Testing and Materials, Philadelphia, Pa. Part 17, p. 111.
29. Marshall, D. B. (1980). *Bull. Am. Ceram. Soc.* **59**, 551.
30. Marshall, D. B. & Lawn, B. R. (1981). *Comm. Am. Ceram. Soc.* In press.